

Continuous Quantum Measurements via Random-Time Sampling

Markus Sifft¹ and Daniel Hägele¹

¹*Ruhr University Bochum, Faculty of Physics and Astronomy, Experimental Physics VI (AG), Germany*

(Dated: July 8, 2022)

Random-time sampling of a quantum system is introduced as a new approach to continuous quantum measurements with prospects for ultra-low-perturbation measurements. Random sampling is, e.g., naturally realized in an optical spin noise experiment when weak probe-laser light exhibits random single-photon events in the detector. We show that a direct evaluation of these detector time-traces yields power spectra that are equivalent to those of the usual continuous measurement regime. Surprisingly, this holds true even for average sampling rates much lower than the typical frequency range of the measured quantum dynamics. The third-order quantum polyspectrum (bispectrum) also contains the same information as its continuous counterpart. Many applications of random-time sampling are envisioned for high-resolution spectroscopy, circuit quantum electrodynamics, quantum sensing, and quantum measurements in general.

Probing of quantum systems is at the heart of quantum technologies for current and future applications in quantum sensing [1], quantum information [2], and quantum measurements in general [3]. Backaction of the measurement on the system is a major problem even of quantum-limited probing. Pfender *et al.* recently introduced a scheme of sequential instead of continuous weak measurements to dramatically reduce the influence of their probe system resulting in high-resolution spectra of the quantum system [4]. However, such undersampling schemes cause multiple replicas of original lines in the spectra as artifacts, which compromise applications where several distant frequencies of the systems have to be probed. Here we introduce random-time sampling of system dynamics as a new way of accessing quantum dynamics. Our numerics shows that power spectra and bispectra [5] directly calculated from traces of random-time quantum measurements are fully equivalent to those from usual continuous quantum measurements. Surprisingly, this holds true even for average sampling rates below the frequencies of the system dynamics. Apart from carefully devised random-time measurement schemes, random sampling can naturally occur if the probe itself shows quantum behavior. A weak probe laser beam in a spin noise experiment [6], e.g., will lead to random Poisson distributed click events in a photomultiplier tube. Our theory includes for the first time a quantum mechanical description of spin noise spectroscopy at low probe photon rates complementing earlier theories [7, 8].

Random-time sampling is inspired from classical signal processing [9–11]: Consider the autocorrelation of a stationary continuous random process $x(t)$

$$g_x(\tau) = \langle x(t + \tau)x(t) \rangle, \quad (1)$$

which yields the power spectrum via Fourier transformation according to the Wiener-Khinchin theorem. The angle brackets relate to the expectation value (here, the temporal average). Random-time sampling is described by a sum of Dirac-delta functions $y(t) = \sum_j \delta(t - t_j)$ where the times t_j are Poisson distributed at an average

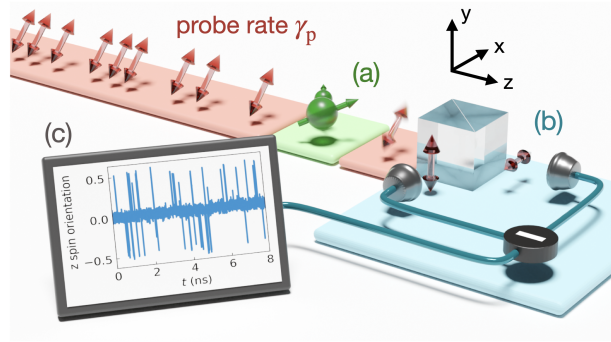


FIG. 1. Schematics of random-time sampling. The linearly polarized probe photons (red double arrows) arrive at random times in the interaction region where they interact and entangle with the quantum system (a) and may weakly change their orientation (blurred double arrow). After traversing the polarizing beamsplitter a photon with either horizontal or vertical polarization causes an event in the corresponding detector (b) giving rise to a positive or negative peak in the measurement trace (c).

rate $\gamma_p = \langle y(t) \rangle$. The random process $z(t) = x(t)y(t)$ represents the result of a random time-sampling of $x(t)$. Its autocorrelation

$$\begin{aligned} g_z(\tau) &= \langle x(t + \tau)y(t + \tau)x(t)y(t) \rangle \\ &= \langle x(t + \tau)x(t) \rangle \langle y(t + \tau)y(t) \rangle \\ &= g_x(\tau)[\gamma_p \delta(\tau) + \gamma_p^2] \end{aligned} \quad (2)$$

follows after noting that x and y are independent and therefore allow for the factorization in the second line. The result for g_z is equivalent to g_x except at $\tau = 0$. The discrepancy results only in an additional flat background contribution to the power spectrum of $z(t)$ in comparison with the spectrum of $x(t)$. A reconstruction of g_x from g_z does not depend on γ_p and is possible even for average sampling rates below the frequency range of $x(t)$. Third-order moments and the corresponding bispectrum of $z(t)$ have been treated as late as 2006 [11]. The bispectrum of $z(t)$ contains the desired bispectrum of $x(t)$ and four

additional terms whose simple structure, however, allows for their subtraction.

It is not immediately clear if the success of classical random sampling can be repeated in the quantum case of sampling with single photons. While the peaks in the classical $z(t)$ are scaled with $x(t)$, a single photon event in a detector contains no quantitative information on the quantum system. However, its probability to appear will depend on the actual state of the quantum system.

A quantum mechanical model of random sampling Our theory of quantum measurements via random-sampling is based on recent progress in *continuous* measurement theory [12–14] regarding exact analytical expressions for multi-time moments and quantum polyspectra of the detector output $z(t)$ [5, 8, 15]. The so-called stochastic master equation (SME) specifies the system Hamiltonian H and the measurement operator A as well as coupling to the environment and the strength of the continuous measurement [16]. The time-trace $z(t)$ can be thought of as the result of a continuous stream of weak probing events that yield an estimate for the expectation value of A on a Gaussian noise background [17]. In order to describe *random-time* sampling, the probe system (e.g. a photon with two polarization states or an electron spin) is here explicitly included in the overall quantum system described by H . The probe system enters incoherently an interaction region (a) with the quantum system at a certain rate γ_p (Fig. 1). The probe system may slightly change its state due to interaction with the quantum system, thus gaining some knowledge about the quantum system. At the same time, the quantum system gets perturbed by the probe system (measurement backaction). The probe system leaves the interaction region at a rate γ_{out} towards the detector region (b) where a strong continuous measurement on the probe system (e.g. of its polarization state) is modeled via the standard SME. The detector region is left towards the environment at a rate γ_{det} . For $\gamma_p \ll \gamma_{\text{out}}$ and $\gamma_{\text{out}} \approx \gamma_{\text{det}}$, the time-dependent occupation of the detector region shows typical Poisson behavior (like clicks of a random radioactive decay).

The overall Hamiltonian H consists of the quantum system (s) and its interaction with the probe system

$$H = H_s + H_{\text{int}}, \quad (3)$$

where H_s may be any system Hamiltonian. We employ a simple linear interaction

$$H_{\text{int}} = \hbar g s_z a_z, \quad (4)$$

where g corresponds to the interaction strength, s_z relates to some property of the system (e.g. the z -component of the spin of one of its electrons), and a_z relates to the z -component of the probe spin (analogous to photon angular momentum) in the interaction region (a). Note, that the probe system in the interaction region is described by three states: $|a_{z,\uparrow}\rangle$, $|a_{z,\downarrow}\rangle$, and the empty

state $|a_0\rangle$. The operator a_z thus reads in that basis

$$a_z = \begin{pmatrix} 1/2 & 0 & 0 \\ 0 & -1/2 & 0 \\ 0 & 0 & 0 \end{pmatrix}, \quad (5)$$

where we recognize the Pauli spin operator for the z -direction. The operators a_x and a_y follow in analogy to the other Pauli spin operators. The operators b_z , b_x , and b_y for the probe system in the detector region have the same representation in their basis as the a_j s. The system dynamics given by the density matrix $\rho(t)$ is governed by the SME (Ito-calculus) [16]

$$\begin{aligned} d\rho = & \frac{i}{\hbar} [\rho, H] dt + \gamma_p \mathcal{D}[d_a](\rho) dt + \gamma_{\text{out}} \mathcal{D}[d_{ab}](\rho) dt \\ & + \gamma_{\text{det}} (\mathcal{D}[d_{b,\uparrow}](\rho) + \mathcal{D}[d_{b,\downarrow}](\rho)) dt \\ & + \beta^2 \mathcal{D}[A](\rho) dt + \beta \mathcal{S}[A](\rho) dW \end{aligned} \quad (6)$$

with the damping terms

$$\mathcal{D}[c](\rho) = c\rho c^\dagger - (c^\dagger c\rho + \rho c^\dagger c)/2 \quad (7)$$

and backaction term

$$\mathcal{S}[c](\rho) = c\rho + \rho c^\dagger - \text{Tr} [(c + c^\dagger)\rho] \rho, \quad (8)$$

where we used the notation of [15] and [5]. The differential dW relates to a stochastic Wiener-process, where $\Gamma(t) = dW(t)/dt$ is white Gaussian noise, i.e. $\langle \Gamma(t)\Gamma(t') \rangle = \delta(t - t')$. The resulting detector output is given by

$$z(t) = \beta^2 \text{Tr}[\rho(t)(A + A^\dagger)/2] + \beta \frac{1}{2} \Gamma(t) \quad (9)$$

as the system is monitored with the measurement operator $A = b_y$ and the measurement strength β . The probe system entering the interaction region in state $|a_{x,\uparrow}\rangle$ is modeled in the SME via the superoperator $\mathcal{D}[d_a]$ with

$$d_a = \mathbb{1}_s \otimes |a_{x,\uparrow}\rangle \langle a_0| \otimes \mathbb{1}_b. \quad (10)$$

Similarly, the spin/polarization-conserving transition from region (a) to (b) is modeled via

$$\begin{aligned} d_{ab} = & (\mathbb{1}_s \otimes |a_0\rangle \langle a_{x,\downarrow}| \otimes \mathbb{1}_b) \cdot (\mathbb{1}_s \otimes \mathbb{1}_a \otimes |b_{x,\downarrow}\rangle \langle b_0|) \\ & + (\mathbb{1}_s \otimes |a_0\rangle \langle a_{x,\uparrow}| \otimes \mathbb{1}_b) \cdot (\mathbb{1}_s \otimes \mathbb{1}_a \otimes |b_{x,\uparrow}\rangle \langle b_0|). \end{aligned} \quad (11)$$

The probe system leaves the detector via

$$d_{b,\uparrow/\downarrow} = \mathbb{1}_s \otimes \mathbb{1}_a \otimes |b_0\rangle \langle b_{z,\uparrow/\downarrow}|. \quad (12)$$

After introducing the Liouvillian $\mathcal{L}[\beta]$ the SME reduces to

$$d\rho = \mathcal{L}[\beta](\rho) dt + \beta \mathcal{S}[A](\rho) dW. \quad (13)$$

Next, we give an illustrative example of a random-time measurement on a single electron spin that is precessing in an external magnetic field B parallel to the x -direction,

$$H_s = \hbar\omega_L s_x, \quad (14)$$

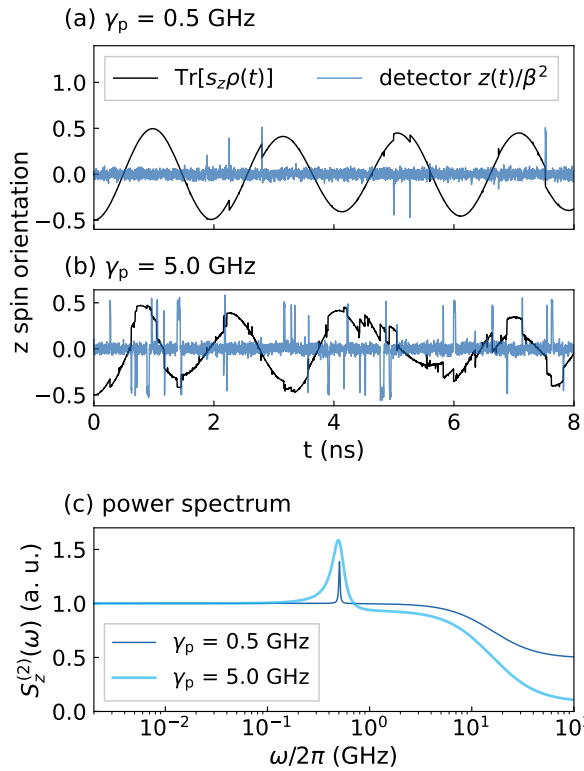


FIG. 2. (a) Detector output shows single probe events (blue line) at low sampling rates while the system exhibits an almost coherently precessing spin (black line). (b) The spin precession shows stronger perturbations at elevated average sampling rates. (c) Corresponding power spectra of the detector output for low and elevated average sampling rates.

where ω_L is the Larmor frequency.

The z -direction of the electron spin is probed by a stream of single photons linearly polarized in xy -direction (Fig. 1). The two circular polarization states of the probe photon can be treated in full analogy to spin 1/2 up and down states in z -direction. After interacting with the system (s), the photon polarization axis is slightly rotated in the xy -plane depending on the z -spin orientation (Faraday-effect). The photon polarization is then measured in y -direction and x -direction via a strong continuous measurement (large β) which mimics a setup consisting of a polarizing beam splitter and a pair of photomultipliers. The detector output $z(t)$ will exhibit either a strong positive or a strong negative peak. Without interaction their probability of appearance is 50 % each. The probabilities slightly change if the system alters the photon's polarization state in the interaction region. The measurement result, therefore, contains some (but not full) information about the z -spin orientation at the time of interaction. Figure 2(a) shows the detector output $z(t)$ found from numerical integration of Eq. (13) for $\omega_L/2\pi = 0.509$ GHz, $g = 100$ GHz, $\gamma_p = 0.5$ GHz, $\gamma_{\text{out}} = 100$ GHz, $\gamma_{\text{det}} = 100$ GHz, and $\beta^2 = 10^4$ GHz. In

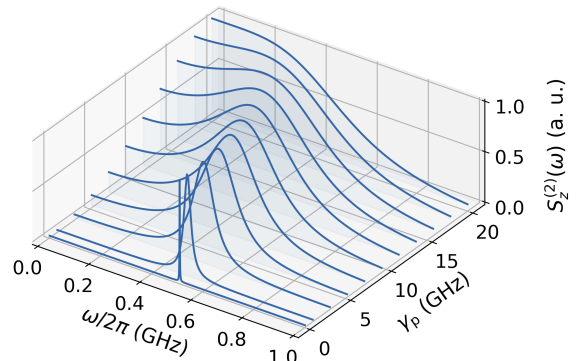


FIG. 3. Power spectra of the detector output for increasing average sampling rates γ_p of a precessing electron spin show a clear Zeno transition with suppression of precession dynamics for highest rates.

a spin noise experiment with a laser probe at 800 nm, a photon rate $\gamma_p = 0.5$ GHz corresponds to a light power of 0.12 nW. Peaks, both positive and negative, related to photon detection events are clearly visible in $z(t)$ on an otherwise Gaussian background noise. The peaks vary in height and widths closely resembling actual current traces of photomultiplier tubes. The expectation value $\text{Tr}(s_z \rho(t))$ of the spin z -component displays a coherent precession dynamics that is only weakly disturbed at the times of a photo detection event. At an increased average rate $\gamma_p = 5.0$ GHz of the incoming probe system, the precession dynamics is clearly distorted [Fig. 2(b)].

For the analysis of actual experiments, the power spectra $S_z^{(2)}(\omega)$ can be directly estimated from the experimental $z(t)$ (see App. B of [5]) without the need for introducing thresholds or counters for signal conditioning. Roughly speaking, the power spectrum $S_z^{(2)}(\omega)$ is via the Fourier transformation of $z(t)$ strongly related to the expectation value $\langle z(\omega) z^*(\omega) \rangle$. Here, we evaluate the general analytical expression for powerspectra $S_z^{(2)}(\omega)$ which is given in terms of the Liouvillian $\mathcal{L}[\beta]$ and the measurement operator A (see Eq. (111) and Sec. XV in [8]). The spectrum in Fig. 2(c) for $\gamma_p = 0.5$ GHz shows a broad Lorentzian background originating from the single photon events and a peak at the Larmor frequency ω_L . For $\gamma_p = 5.0$ GHz the peak exhibits a clear broadening and small shift to lower frequencies as expected for oscillations with increased damping. Fig. 3 shows the power spectra for increasing measurement rates γ_p where background has been subtracted using power spectra for the case of no probe-interaction with the system, $H_{\text{int}} = 0$. At high rates the spectrum broadens and shifts to zero frequencies as the frequent measurements suppress all coherent dynamics. This behavior is known as quantum Zeno effect [18]. Korotkov studied the Zeno transition using a continuous measurements approach. He found the same spectral features as in our case of random sam-

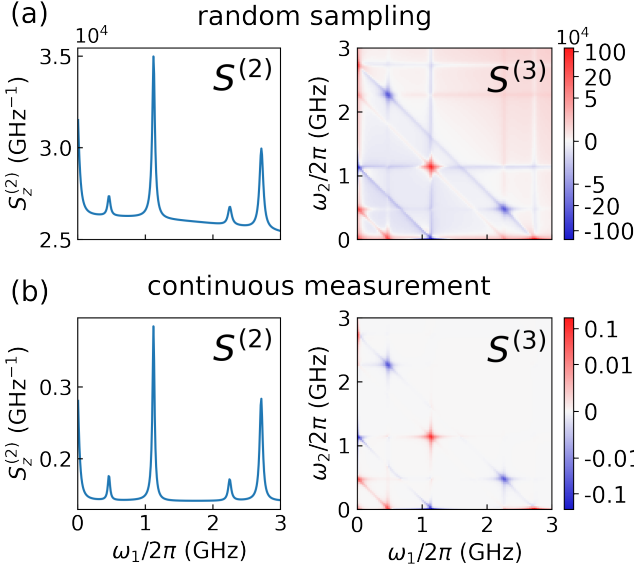


FIG. 4. (a) Power spectrum $S_z^{(2)}(\omega)$ and bispectrum $S_z^{(3)}(\omega_1, \omega_2)$ of the z -component of one spin in a coupled spin system measured via random sampling. An average background of $-4.04 \times 10^4 \text{ GHz}^{-2}$ was subtracted. (b) The spectra in the case of a continuous quantum measurement closely resemble that of case (a) except for the background and stripes. The color bar is scaled via the arsinh-function.

pling [19].

Our numerics for γ_p down to 0.05 GHz suggests that the width of the spectrum scales for lower rates linearly with γ_p allowing for the detection of a fully coherent oscillation in the limit $\gamma_p \rightarrow 0$, i.e. reaching an ultra-weak measurement limit. An analytical proof for this behavior is, however, still missing.

Bispectrum of a two-spin system We study two coupled spins that are precessing inside a tilted magnetic field. Such non-trivial systems are known to exhibit several peaks in the second-order spectrum. Moreover, higher-order correlations can be found in the third-order quantum polyspectrum (bispectrum) [8]. The so-called bispectrum $S_z^{(3)}(\omega_1, \omega_2)$ is related to $\langle z(\omega_1)z(\omega_2)z^*(\omega_1+\omega_2) \rangle$ (exact definition see [20]). Bispectra of quantum measurements have been used for evaluating transport experiments in nano-electronics [5, 21] and for the analysis of non-Gaussian dephasing environments in circuit quantum electrodynamics (cQED) [22]. The quantum system is defined by

$$H_s = \hbar\omega_L^{(1)}(\sin(\varphi)s_x^{(1)} + \cos(\varphi)s_z^{(1)}) + \hbar\omega_L^{(2)}(\sin(\varphi)s_x^{(2)} + \cos(\varphi)s_z^{(2)}) + g_c[s_x^{(1)}s_x^{(2)} + s_y^{(1)}s_y^{(2)} + s_z^{(1)}s_z^{(2)}], \quad (15)$$

where $\omega_L^{(1)}/2\pi = 1.592 \text{ GHz}$, $\omega_L^{(2)}/2\pi = 0.0 \text{ GHz}$, $g_c = 10 \text{ GHz}$, and $\varphi = \pi/6$ is the tilt-angle of the magnetic field. $H_{\text{int}} = \hbar g s_z^{(1)} a_z$, where $g = 50 \text{ GHz}$, $\gamma_p = 5 \text{ GHz}$,

$\gamma_{\text{out}} = 100 \text{ GHz}$ and $\beta^2 = 10^4 \text{ GHz}$. An additional spin relaxation term $\frac{\gamma_s}{2} \mathcal{D}[d_s](\rho)$ with $d_s = |s_{z,\downarrow}^{(1)}\rangle \langle s_{z,\uparrow}^{(1)}| \otimes \mathbb{1}_{s^{(2)}} \otimes \mathbb{1}_a \otimes \mathbb{1}_b$ is introduced which drives the first spin towards the $-z$ direction at a slow rate $\gamma_s = 0.1 \text{ GHz}$. Consequently, $\langle s_z^{(1)} \rangle < 0$ and $\langle z(t) \rangle < 0$ will hold for the experimental setup. The spectrum $S_z^{(2)}(\omega)$ of the random sampling trace in Figure 4(a) shows several peaks corresponding to quantum beats between different energy eigenstates of the system. The third-order spectrum (Eq. (110) in [8]) exhibits a large negative background (subtracted in the Figure), straight lines that extend to higher frequencies, and several sharp peaks. The peaks only appear in $S_z^{(3)}$ of the usual continuous measurement (Fig. 4(b), where $\beta^2 = 0.5625 \text{ GHz}$ and $A = s_z^{(1)}$ using standard theory [8]). Benhenni and Rachdi show in their classical treatment of bispectra from random sampling that the asymptotic behavior of the additional contributions to $S_z^{(3)}$ makes it possible to separate them from the desired peak structure [11]. After a first attempt we believe that separation of such contributions is also possible in the quantum case. A spectrum without background and stripes was found for $\langle z(t) \rangle = 0$ when $\gamma_s = 0$.

Conclusion Random-time sampling has been introduced as a new spectroscopic tool that is capable of characterizing second- and third-order coherence in quantum dynamics even at very low average sampling rates. Random-time sampling therefore is a viable and more versatile alternative to recently introduced high resolution spectroscopy via sequential weak measurements [4]. Random sampling by single-photon detectors also offers an alternative to amplification schemes via heterodyning in the very active field of spin noise spectroscopy [23–25]. Todays experiments of cQED offer a great control of probe events with desired timing and interaction strength [26, 27]. Especially the investigation of non-Gaussian environmental noise in cQED may benefit from measuring the power spectrum and bispectrum of a detector qubit via random sampling with ultra-weak backaction [22].

We acknowledge financial support by the German Science Foundation (DFG) under Grant No. HA 3003/7-1.

- [1] C. L. Degen, F. Reinhard, and P. Cappellaro, Quantum sensing, *Rev. Mod. Phys.* **89**, 035002 (2017).
- [2] A. Blais, S. A. Girvin, and W. D. Oliver, Quantum information processing and quantum optics with circuit quantum electrodynamics, *Nat. Phys.* **16**, 247 (2020).
- [3] A. A. Clerk, M. H. Devoret, S. M. Girvin, F. Marquardt, and R. J. Schoelkopf, Introduction to quantum noise, measurement, and amplification, *Rev. Mod. Phys.* **82**, 1155 (2010).
- [4] M. Pfender, P. Wang, H. Sumiya, S. Onoda, W. Yang, D. B. R. Dasari, P. Neumann, X.-Y. Pan, J. Isoya, R.-B. Liu, and J. Wrachtrup, High-resolution spectroscopy of single nuclear spins via sequential weak measurements,

Nature Commun. **10**, 594 (2019).

[5] M. Sifft, A. Kurzmann, J. Kerski, R. Schott, A. Ludwig, A. D. Wieck, A. Lorke, M. Geller, and D. Hägele, Quantum polyspectra for modeling and evaluating quantum transport measurements: A unifying approach to the strong and weak measurement regime, Phys. Rev. Res. **3**, 033123 (2021).

[6] G. M. Müller, M. Oestreich, M. Römer, and J. Hübner, Semiconductor spin noise spectroscopy: Fundamentals, accomplishments, and challenges, Physica E **43**, 569 (2010).

[7] N. A. Sinitzyn and Y. V. Pershin, The theory of spin noise spectroscopy: a review, Rep. Prog. Phys. **79**, 106501 (2016).

[8] D. Hägele and F. Schefczik, Higher-order moments, cumulants, and spectra of continuous quantum noise measurements, Phys. Rev. B **98**, 205143 (2018).

[9] H. S. Shapiro and R. A. Silverman, Alias-free sampling of random noise, J. Soc. Ind. Appl. Math. **8**, 225 (1960).

[10] G. Pasini, P. A. Traverso, D. Mirri, G. Iculano, and F. Filicori, Hardware implementation of a broad-band vector spectrum analyzer based on randomized sampling, IEEE Trans. Instr. Meas. **54**, 1575 (2005).

[11] K. Benhenni and M. Rachdi, Bispectrum estimation for a continuous-time stationary process from a random sampling, in *Recent advances in stochastic modelling and data analysis*, edited by C. H. Skiadas (Word Scientific, 2007) p. 442.

[12] Y. Aharonov, D. Z. Albert, and L. Vaidman, How the result of a measurement of a component of the spin of a spin-1/2 particle can turn out to be 100, Phys. Rev. Lett. **60**, 1351 (1988).

[13] L. Diosi, Continuous quantum measurement and Ito formalism, Phys. Lett. A **129**, 419 (1988).

[14] A. Barchielli and M. Gregoratti, *Quantum Trajectories and Measurements in Continuous Time: The Diffusive Case*, Lecture Notes in Physics 782 (Springer, Berlin Heidelberg, 2009).

[15] A. Tilloy, Exact signal correlators in continuous quantum measurements, Phys. Rev. A **98**, 010104(R) (2018).

[16] K. Jacobs and D. A. Steck, A straightforward introduction to continuous quantum measurement, Contemp. Phys. **47**, 279 (2006).

[17] J. Gross, C. Caves, G. Milburn, and J. Combes, Qubit models of weak continuous measurements: Markovian conditional and open-system dynamics, Quantum Science and Technology **3**, 024005 (2018).

[18] B. Misra and E. C. G. Sudarshan, The zeno's paradox in quantum theory, J. Math. Phys. **18**, 756 (1977).

[19] A. N. Korotkov, Output spectrum of a detector measuring quantum oscillations, Phys. Rev. B **63**, 085312 (2001).

[20] D. R. Brillinger, An introduction to polyspectra, Ann. Math. Statist. **36**, 1351 (1965).

[21] N. Ubbelohde, C. Fricke, C. Flindt, F. Hohls, and R. J. Haug, Measurement of finite-frequency current statistics in a single-electron transistor, Nat. Commun. **3**, 612 (2012).

[22] L. M. Norris, G. A. Paz-Silva, and L. Viola, Qubit noise spectroscopy for non-Gaussian dephasing environments, Phys. Rev. Lett. **116**, 150503 (2016).

[23] S. Cronenberger and D. Scalbert, Quantum limited heterodyne detection of spin noise, Rev. Scientific Instrum. **87**, 093111 (2016).

[24] P. Sterin, J. Wiegand, J. Hübner, and M. Oestreich, Optical amplification of spin noise spectroscopy via homodyne detection, Phys. Rev. Appl. **9**, 034003 (2018).

[25] A. N. Kamenskii, M. Y. Petrov, G. G. Kozlov, V. S. Zapasskii, S. E. Scholz, C. Sgroi, A. Ludwig, A. D. Wieck, M. Bayer, and A. Greilich, Detection and amplification of spin noise using scattered laser light in a quantum-dot microcavity, Phys. Rev. B **101**, 041401(R) (2020).

[26] Q. Ficheux, S. Jezouin, Z. Leghtas, and B. Huard, Dynamics of a qubit while simultaneously monitoring its relaxation and dephasing, Nature Commun. **9**, 1926 (2018).

[27] Z. K. Minev, S. O. Mundhada, S. Shankar, P. Reinhold, R. Gutierrez-Jauregui, R. J. Schoelkopf, M. Mirrahimi, H. J. Carmichael, and M. H. Devoret, To catch and reverse a quantum jump mid-flight, Nature **570**, 200 (2019).